NANO LETTERS

2007
Vol. 7, No. 3
614−619

Translocation of C_{60} and Its Derivatives Across a Lipid Bilayer

Rui Qiao*

Department of Mechanical Engineering, Clemson University, Clemson, South Carolina 29634

Aaron P. Roberts

Department of Biological Sciences, University of North Texas, Institute of Applied Science, UNT, Denton, Texas 76203

Andrew S. Mount and Stephen J. Klaine

College of Agriculture, Forestry and Life Sciences, Clemson University, Clemson, South Carolina 29634

Pu Chun Ke

Department of Physics and Astronomy, Clemson University, Clemson, South Carolina 29634

Received October 25, 2006; Revised Manuscript Received January 24, 2007

ABSTRACT

Obtaining an understanding, at the atomic level, of the interaction of nanomaterials with biological systems has recently become an issue of great research interest. Here we report on the molecular dynamics study of the translocation of fullerene C_{60} and its derivative $C_{60}(OH)_{20}$ across a model cell membrane (dipalmitoylphosphatidylcholine or DPPC bilayer). The simulation results indicate that, although a pristine C_{60} molecule can readily *"jump"* into the bilayer and translocate the membrane within a few milliseconds, the $C_{60}(OH)_{20}$ molecule can barely penetrate the bilayer. Indeed, the mean translocation time via diffusion for the $C_{60}(OH)_{20}$ molecule is several orders of magnitude longer than for the former. It was also determined that the two different forms of fullerenes, when adsorbed into/onto the bilayer, affected the membrane structure differently. This study offers a mechanistic explanation of that difference and for the reduced acute toxicity of functionalized fullerenes.

Nanomaterials, whose dimensions range from 1 to 100 nm, can exhibit drastically different characteristics compared to their bulk counterparts. Although the use of such materials in biological systems opens avenues for the creation of novel biosensing and alternative nanomedical technologies, these nanomaterials can also be highly toxic. A greater understanding of the interaction of nanomaterials with biological systems, especially of the interaction of nanomaterials with cell membranes, will enable us to take full advantage of the unique properties of nanomaterials while minimizing their adverse effects.

Fullerenes and their derivatives are an important subset of nanomaterials. Fullerenes C_{60}, C_{70}, and their water-soluble derivatives have been used as robust oxygen scavengers,[1] anti-HIV drugs,[2] X-ray contrast agents,[3] and transporters for delivering the murine anti-gp240 melanoma antibody.[4−8] Extensive photophysical studies over the past decade have shown that C_{60} and C_{70} in their ground states and in their triplet energy states can facilitate the transport of electrons across the bilayer for enhanced photosynthesis and a theoretical reduction in the yield of reactive oxygen species associated with mitochondria activities in cells.[7]

Though the existing studies on the interactions of C_{60} with cell membranes are limited, it has been suggested that the accumulation of C_{60} in a DPPC bilayer may cause degradation and a suppression of the phase transitions of the host bilayer.[9] Recently, Colvin's group determined that the toxicity of pristine C_{60} can cause membrane leakage.[10] They also found that the functionalization of C_{60} dramatically lowered toxicity with no resultant membrane leakage. However, studies of these atomistic processes have only received recent attention[11,12] and the effects of surface functionalization have yet to be addressed. This paper details our study of the interaction of pristine and functionalized C_{60} with a lipid bilayer and the subsequent translocation of these fullerenes using molecular dynamics simulations.

* Corresponding author. Email: rqiao@ces.clemson.edu. URL: http://www.clemson.edu/~rqiao.

10.1021/nl062515f CCC: $37.00
Published on Web 02/23/2007

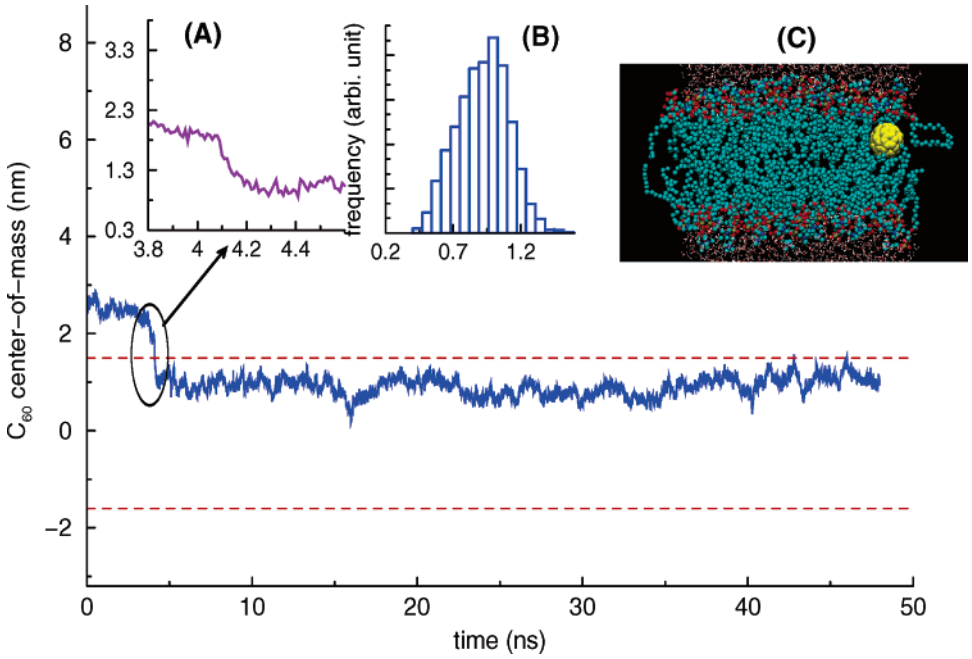

Figure 1. Trajectory of the C_{60} molecule in the transmembrane (z) direction. The two dashed lines denote the locations of density peaks of the upper and lower leaflet of the DPPC bilayer. (A) Zoomed view of the trajectory at $t \approx 4.09$ ns. (B) Histogram of the z-coordinate of the center-of-mass of C_{60} molecule after the buckyball enters the bilayer ($t > 4.2$ ns). (C) Side view of the simulation system at $t = 34.5$ ns. The yellow ball denotes the C_{60} molecule, cyan dots denote the lipid tail groups, and the red and blue dots represent the lipid head groups. The snapshot was rendered using VMD.[21]

Simulation Details. The simulation system that we developed consists of 128 fully hydrated dipalmitoylphosphatidylcholine (DPPC) lipid molecules and one C_{60} or $C_{60}(OH)_{20}$ molecule. There are 5486 and 5536 water molecules in the system containing a C_{60} and a $C_{60}(OH)_{20}$ molecule, respectively. The initial configuration of the bilayer was obtained from a previous equilibrium simulation by Tieleman and Berendsen.[13] The bilayer is in the xy-plane and the middle plane of the bilayer was initially located at $z = 0$. The C_{60} and $C_{60}(OH)_{20}$ molecules were placed at $z = 2.8$ and 4.7 nm, respectively. Visual inspection indicated that they are not in contact with the lipid molecules.

The force field for the DPPC molecules is the same as that used in refs 14 and 15, which has been extensively validated. Water is modeled by using the SPC model. C_{60} is modeled as a rigid body with a C−C bond length of 1.46 Å. $C_{60}(OH)_{20}$ is modeled by attaching OH groups to 20 carbon atoms distributed approximately uniformly on the pristine C_{60} molecule. The C−O and O−H bond lengths are 1.40 and 0.95 Å, respectively.[16] The C−O−H bond angle is 106.3°.[16] The carbon atoms of the C_{60} are modeled as neutral. In the $C_{60}(OH)_{20}$ molecule, the oxygen and hydrogen atoms are assigned partial charges of $-0.8e$ and $+0.3e$, respectively, and the carbon atoms directly connected to the oxygen atoms are each assigned a partial charge of $+0.5e$. The Lennard-Jones parameters (van der Waals diameter σ and interaction strength ϵ) for the carbon atoms same as that used in ref 17.

Simulations were performed in the NPT ensemble by using the Gromacs package.[18,19] The temperature of the system was coupled to a Berendsen thermostat (temperature 325 K, time constant 0.1 ps) and the pressure was coupled semi-isotropically to a Berendsen barostat (pressure 1 bar, time constant 0.5 ps). The Lennard-Jones potentials were computed by using a cutoff length of 1.0 nm, and the electrostatic interactions were computed by using the PME method (real space cutoff 1.0 nm, FFT grid spacing 0.12 nm). The lengths of all bonds were kept constant using the Lincs algorithm.[20] The time step for simulations was 2 fs. A pre-equilibrium run of 2 ns was first performed, followed by a production run of 48 ns.

Simulation Results: Pristine C_{60}. Figure 1 shows the evolution of the z-position of the C_{60} molecule. The boundaries of the bilayer in the z-direction, defined as the two peaks of lipid density (each corresponding to a leaflet of the bilayer), are $z = \pm 1.5$ nm and are labeled in the same figure. We observed that the C_{60} molecule initially diffuses slowly toward the bilayer. However, at $t \approx 4.09$ ns, the C_{60} molecule virtually "jumped" into the lipid bilayer. Such a jump is shown more clearly in the inset A of Figure 1, and the average speed of the jump was calculated to be ~10 m/s by assuming that the jump occurred during $t = 4.08$ to 4.15 ns. Once the C_{60} molecule moved into the lipid bilayer, it remained in the lipid bilayer for the rest of the simulation. We repeated the simulation with a different initial configuration, and fast "jump" with a speed of ~6 m/s was observed. Inset B shows a histogram of the z-position of C_{60} molecule after it enters the bilayer, and we observed that the most probable z-positions of the C_{60} molecule is $z \approx 1.0$ nm. Inset C illustrates a snapshot of the simulation system at $t = 34.5$ ns, and we found that the C_{60} molecule adsorbed deeply in the bilayer was wrapped by the lipid tails.

The adsorption of C_{60} molecule into the lipid bilayer is driven by the hydrophobic interactions between the C_{60} and the lipid tails. To obtain a more quantitative picture of these

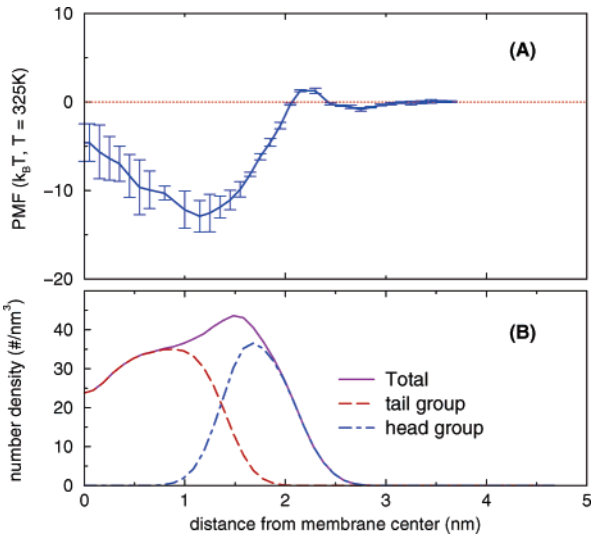

Figure 2. (A) Potential of mean force (PMF) of pristine C_{60} as a function of its distance from the central plane of the DPPC bilayer. Because of the symmetry with respect to the central plane of the bilayer, only the PMF profile in the upper leaflet of the bilayer is shown. (B) Number density profile of the DPPC bilayer. All atoms except the hydrogen atom are counted.

interactions, we performed additional simulations to compute the potential of mean force (PMF) of the C_{60} molecule at different transmembrane positions. The C_{60} molecule was fixed at different *z*-positions and we computed the average force acting on it during the simulation. For each of these simulations, a 3 ns equilibrium was first performed so that the system reached equilibrium, and this was followed by a 4 ns simulation during which the average force was calculated. Such a method was discussed in ref 22 and has been used previously to calculate the mean force for ions inside a nanochannel.[23] A mean force was defined as negative if it pulled the C_{60} molecule toward the membrane center. The PMF was obtained by integrating the mean force from bulk (taken as 3.5 nm from the membrane central plane in the current calculation) where the PMF was taken as zero.

Figure 2A shows the PMF of C_{60} as a function of its distance from the central plane of the DPPC bilayer. We observed that the PMF is $-12.9\ k_BT$ at a position 1.1 nm from the bilayer center (k_B = Boltzmann constant; T = system temperature). In addition, a shallow local minimum of PMF was observed outside the bilayer at $z = 2.7$ nm. This PMF profile differs from previous studies which indicated that the PMF minimum is located at the bilayer center ($z = 0$) where the free volume is the largest.[24] However, the PMF in Figure 2 shows that the lowest PMF is located at $z \approx 1.1$ nm, with a PMF barrier of approximately $8\ k_BT$ between $z \approx 0$ and 1.1 nm. Such an energy barrier is supported by the histogram shown in inset B of Figure 1, which shows that the most probable position inside bilayer is $z \approx 1.0$ nm rather than $z = 0$. We also performed a simulation in which a buckyball was released from $z = 0$ at the beginning of the simulation. It was observed that the buckyball migrated to $z \approx 1.0$ nm within 500 ps and stayed close to that location thereafter. Although these simulations lend certain support to the PMF calculation, they are not rigorous corroborations. To understand the origin of this PMF barrier, we note that the PMF of a finite size object at any position can be computed by summing up energy gain (or cost) during the process of (I) vacating the space to be occupied by the object and (II) inserting the object into the vacancy. Though step I results in a significant cost in energy (especially when the space to be vacated is densely filled with atoms), step II usually results in a gain in energy due to the interactions between the inserted object and its surroundings. The lipid density is lower at $z = 0$ than at $z = 1.1$ nm, implying that both the energy cost for vacating space for a buckyball and the energy gain (due to the van der Waals interactions between the buckyball and its surrounding lipids) of inserting a buckyball are higher at $z = 1.1$ nm. If the energy gain during step II is significantly higher at $z = 1.1$ nm than at $z = 0$, the PMF at $z = 1.1$ nm can be lower than that at $z = 0$. In previous studies on the permeation of a hydrophobic object through a bilayer,[24] a hydrophobic sphere was modeled as a *single* Lennard-Jones atom with interaction parameter ϵ same as that of the oxygen atom. Using such a model, the energy gain during step II is small. For example, the interaction energy between a Lennard-Jones sphere ($\sigma = 1.1$ nm $\approx$ van der Waals diameter of a buckyball) located at $z = 0$ and 1.1 nm with the surrounding was found to be -33.4 ± 5.6 and -40.2 ± 8.3 kJ/mol, respectively. Because the difference of energy gain at these two positions for step II is so small, the PMF difference at these two positions is dominated by the energy cost difference in step I. Therefore, as shown in ref 24, the PMF at $z = 0$ is lower compared to that at $z = 1.1$ nm. However, when the buckyball is explicitly modeled as 60 atoms, the interaction energy is found to be -195 ± 11 and -239 ± 12 kJ/mol, respectively. Here the energy gain of step II at $z = 1.1$ nm is significantly higher than at $z = 0$. Consequently, the PMF becomes lower at $z = 1.1$ nm.

The adsorption of small hydrophobic penetrants into the lipid bilayer is usually hypothesized to be induced by the formation of micropores in the lipid membrane. Here we studied the topology of lipid membrane at $t = 4.09$ ns when the C_{60} was about to "jump" into the lipid bilayer. Figure 3 shows the voronoi tessellation of the top leaflet of DPPC bilayer through which the C_{60} moved into the membrane. We observed that the spacing between lipid heads adjacent to the C_{60} (shown as shaded cells) was large and a pore was formed in the bilayer. The average area per lipid head in the shaded region is 0.80 nm^2, which is approximately 25% larger than the mean value in the entire bilayer.

The translocation of the DPPC bilayer was not observed in our simulation due to the short time scale that can be explored by molecular dynamics simulations. However, with the PMF obtained in Figure 2A, the average time that C_{60} translocates the membrane can be estimated (bounded by $z = \pm 3.5$ nm here) via Brownian diffusion as[25]

$$\langle \tau \rangle = \frac{1}{D_z} \int_{-3.5\text{nm}}^{3.5\text{nm}} e^{\text{PMF}(y)/k_BT}\, dy \int_{-3.5\text{nm}}^{y} e^{-\text{PMF}(z)/k_BT}\, dz \quad (1)$$

where D_z is the diffusion coefficient of C_{60} in the trans-

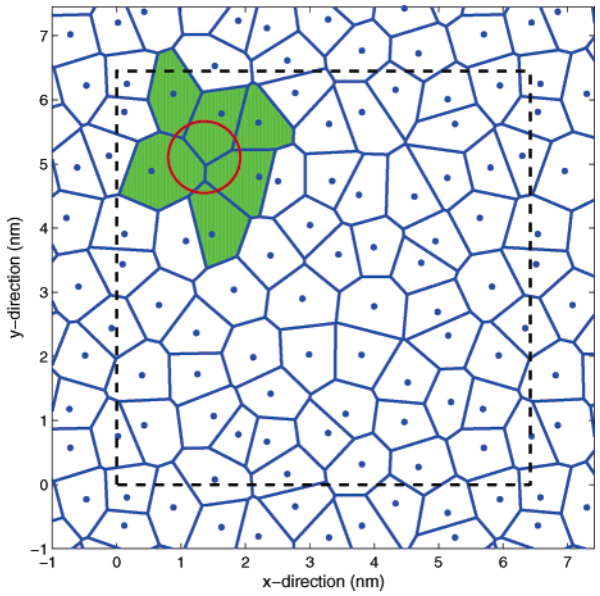

Figure 3. Voronoi tessellation of the top leaflet of DPPC bilayer at $t = 4.09$ ns (i.e., just before the C_{60} molecule "jumps" into the lipid bilayer). Each cell represents a lipid head. The dots denote the center-of-mass of the DPPC head groups and the circle (diameter: 1.2 nm) denotes the projection of C_{60} molecule on the *xy*-plane. The shaded cells correspond to the lipid head groups that are adjacent to the C_{60} molecule. The dashed lines represent the periodic boundary.

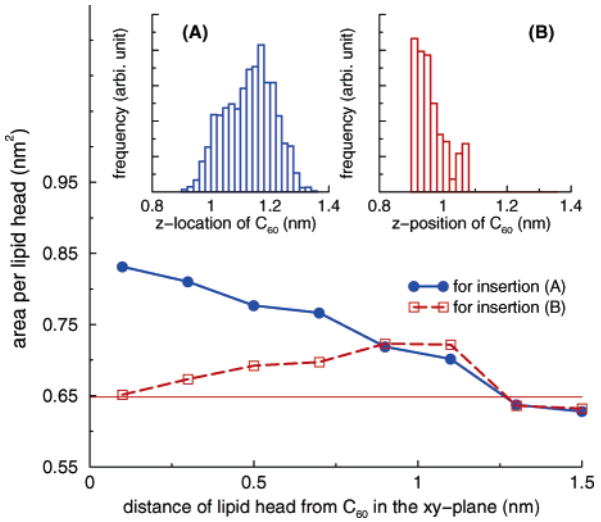

Figure 4. Average area per lipid head as a function of the lateral distance between the lipid head group and the C_{60} molecule adsorbed into the lipid bilayer. The solid line is for time period $t = 19-19.6$ ns, and the dashed line is for time period $t = 19.6-19.9$ ns. The thin red line denotes the average head area of lipid ($A_{av} = 0.648$ nm^2). The histograms of the *z*-coordinate of the C_{60} molecule during these two periods are shown in insets A and B, respectively.

membrane direction. Although the diffusion coefficient of C_{60} is expected to be position-dependent, this variation is not of primary interest here as that of obtaining an order-of-magnitude estimate of $\langle\tau\rangle$. Because the C_{60} mostly inhabits the region $z = 1.1-2.2$ nm during the translocation process, we computed D_z of C_{60} at point $z = 1.7$ nm. Following the method described by Marrink and Berendsen,[24] a D_z of $(2.7 \pm 0.4) \times 10^{-10}$ m/s^2 was obtained. With this D_z and the PMF shown in Figure 2A, the mean translocation time of C_{60} was estimated to be 1.9 ms. Though the translocation of C_{60} into the cell may play an important role in determining the toxic effect of C_{60}-based nanomaterials, existing studies indicate that C_{60} can modify the properties of cell membrane and even induce membrane leakage.[10] The chemical origins of such membrane leakage have been previously proposed;[10] here we explore the possible physical origins of such leakage. Figure 4 shows the average area per lipid head (A_{lipid}) as a function of the lateral distance between the lipid head group and the C_{60} molecule adsorbed into the lipid bilayer during two different time periods. The histogram of the *z*-position of C_{60} molecule during the first time period ($t = 19-19.6$ ns) indicates that the C_{60} is buried relatively shallow in the bilayer, and we observed that A_{lipid} is much higher compared to the average value at positions near the C_{60}. At positions very close to the C_{60}, A_{lipid} is approximately 28% higher than the average value. For C_{60} buried at a slightly deeper position, the variation of A_{lipid} becomes much less significant (<9%). These observations suggest that as the C_{60} diffuses in the lipid bilayers, it can induce local conformational changes. Specifically, when the C_{60} lies close to the surface of the bilayer, it increases the spacing between the lipid head groups, thus facilitating the formation of micropores. The formation of these micropores may enhance the mass transfer of large sized penetrants and cause membrane leakage. The physical mechanism described here can also complement the chemical and biological mechanisms of membrane leakage (e.g., via oxidative damage of lipids).[10] However, the relative importance of the physical mechanism discussed here as compared to the mechanisms reported earlier remains to be elucidated.

Simulation Results:$C_{60}(OH)_{20}$. Figure 5 shows the evolution of the *z*-position of $C_{60}(OH)_{20}$ molecule, and inset A shows the histogram of the *z*-position of the $C_{60}(OH)_{20}$ molecule. We observed that once the $C_{60}(OH)_{20}$ diffused onto the lipid bilayer, it remained on the membrane and did not move into the bilayer during the simulation. Inset B shows a snapshot of the membrane−$C_{60}(OH)_{20}$ complex at $t = 48$ ns. We observed that the $C_{60}(OH)_{20}$ was adsorbed on the head groups of lipid bilayer.

The difficulty for the $C_{60}(OH)_{20}$ to enter the lipid bilayer is mainly due to the fact that functionalization renders the surface of fullerene hydrophilic, thusly favoring its adsorption onto the membrane rather than into the bilayer. To obtain a more quantitative understanding of this phenomenon, we computed the PMF of $C_{60}(OH)_{20}$ across lipid bilayer using the approach described earlier. Only the PMF for $z > 0.95$ nm was calculated because as the $C_{60}(OH)_{20}$ moves into the bilayer, the time necessary for reaching equilibrium dramatically increases making it prohibitively difficult to obtain accurate results. Figure 6 A shows that the PMF exhibits a minimum ($-11.7\ k_BT$) at $z = 2.3$ nm and increases dramatically as $C_{60}(OH)_{20}$ moves toward the bilayer interior. This increase explains the tendency for the $C_{60}(OH)_{20}$ to remain on the surface of lipid membrane instead of entering the bilayer. To estimate the time scale of translocation of $C_{60}(OH)_{20}$ through the DPPC bilayer via Brownian diffusion,

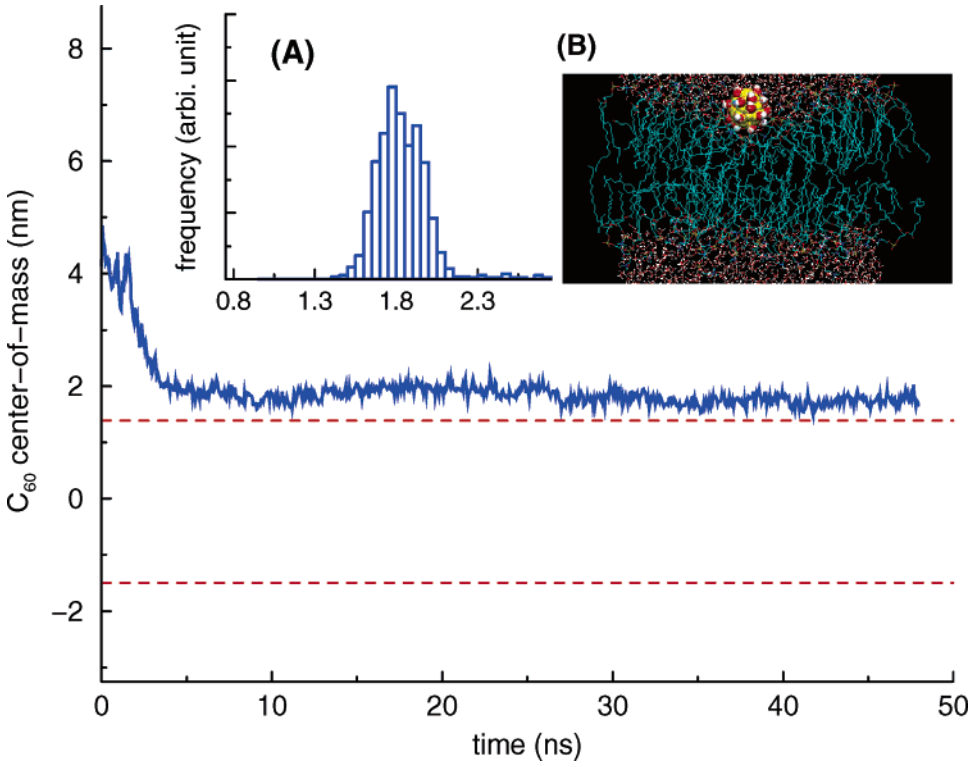

Figure 5. Trajectory of the $C_{60}(OH)_{20}$ molecule in the transmembrane (z) direction. The two dashed lines denote the location of density peak of the upper and lower leaflets of the DPPC bilayer. (A) Histogram of the z-coordinate of the center-of-mass of $C_{60}(OH)_{20}$ molecule during simulation. (B) Representative side view of the simulation system. Yellow balls and the attached large red and white dots denote the $C_{60}(OH)_{20}$ molecule, cyan dots denote the tail groups of the DPPC lipids, and the small red and blue dots denote the lipid head groups.

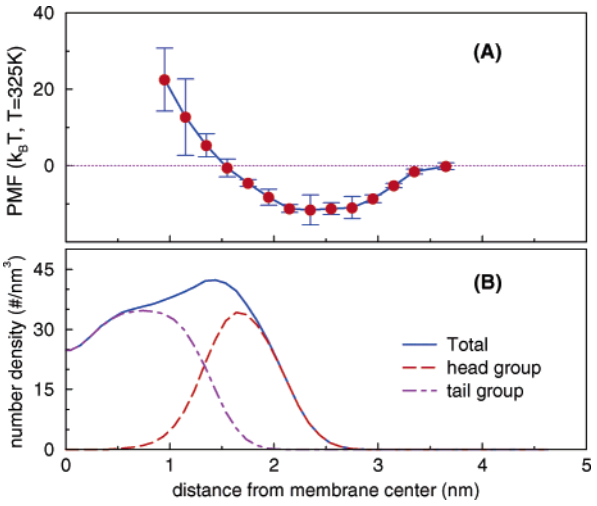

Figure 6. (A) Potential of mean force (PMF) of $C_{60}(OH)_{20}$ as a function of its distance from the central plane of the DPPC bilayer. (B) Number density profile of DPPC bilayer.

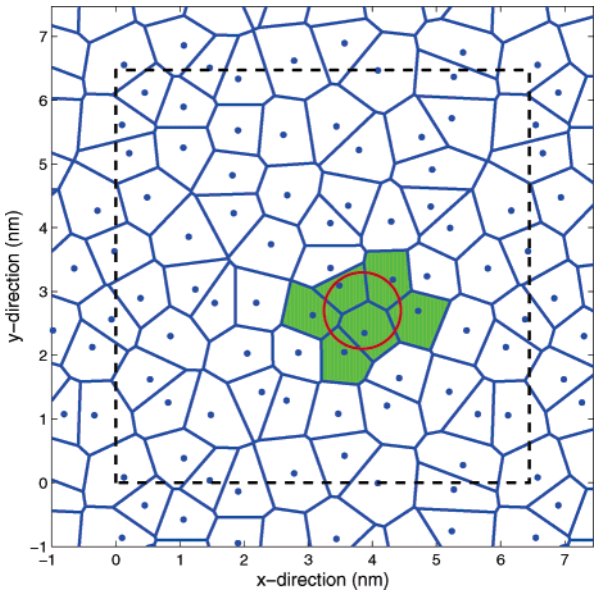

Figure 7. Voronoi tessellation of the top layer of DPPC bilayer at $t = 10.15$ ns. The dots denote the center-of-mass of the DPPC head groups, and the circle (diameter: 1.2 nm) denotes the projection of the $C_{60}(OH)_{20}$ molecule on the xy-plane. The shaded cells denote the lipid head groups that are adjacent to the $C_{60}(OH)_{20}$ molecule. The dashed line denotes the periodic boundary.

we computed the diffusion coefficient of $C_{60}(OH)_{20}$ at $z = 1.25$ nm and obtained a value of $(2.5 \pm 0.3) \times 10^{-10}$ m/s^2. We further assumed that the PMF of $C_{60}(OH)_{20}$ in the region $|z| < 0.95$ nm is the same as $z = 0.95$ nm, which means that the calculated translocation time represents a lower bound of $\langle\tau\rangle$. Using eq 1, the mean translocation time was estimated to be 3×10^6 s, i.e., approximately 9 orders of magnitude larger compared to that for the pristine C_{60}.

Because $C_{60}(OH)_{20}$ prefers to adsorb onto the outer rim of the bilayer, it was found to affect the membrane conformation differently as compared to pristine C_{60}. Figure 7 shows the voronoi tessellation of the top leaflet of a DPPC bilayer at $t = 10.15$ ns. The average lipid head area of lipids near the $C_{60}(OH)_{20}$ (shaded cells in the figure) was 0.52 nm^2, or approximately 20% smaller as compared to the average

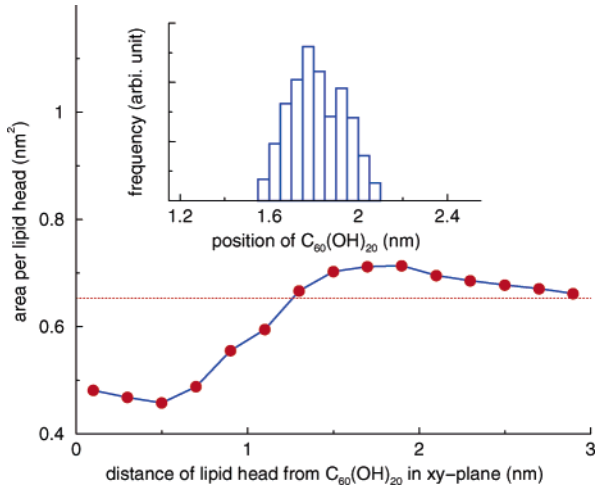

Figure 8. Average area per lipid head as a function of the lateral distance between the head group and the $C_{60}(OH)_{20}$ molecule adsorbed on the top lipid bilayer. The statistics are obtained during the time period of $t = 10-48$ ns. The dashed lines denote the average head area of lipid ($A_{av} = 0.648$ nm^2). Inset: histogram of the z-coordinate of the $C_{60}(OH)_{20}$ molecule during the time period of $t = 10-48$ ns.

lipid head area. Therefore, the $C_{60}(OH)_{20}$ appears to "pinch" the cell membrane. This "pinch" is caused by the strong interactions between the OH groups of $C_{60}(OH)_{20}$ and the lipid head groups. The strong interaction can be inferred from the close proximity of lipid head group to the $C_{60}(OH)_{20}$ adsorbed on the bilayer as shown in Figure 5B.

Figure 8 further shows the average area per lipid head A_{lipid} as a function of the lateral distance between the head group and the $C_{60}(OH)_{20}$ molecule during the time period of $t = 10-48$ ns. As shown in the histogram insertion, $C_{60}(OH)_{20}$ was adsorbed on the lipid membrane in the entire time period. Compared to the situation for pristine C_{60} as shown in Figure 4, A_{lipid} is smaller than the average value at short $C_{60}(OH)_{20}$−lipid distances and increases slightly for distances larger than 1.25 nm. This suggests that the micropore formation is suppressed with the adsorption of $C_{60}(OH)_{20}$ on the lipid membrane. This may be one of the reasons why no membrane leakage was reported for cells in contact with $C_{60}(OH)_{20}$ solution.

In summary, we investigated the interaction of pristine and functionalized C_{60} with a DPPC bilayer using atomistic simulations. We determined that pristine C_{60} molecules can diffuse easily into the bilayer through transient micropores in the membrane, and that the mean translocation time by Brownian diffusion was on the order of a few milliseconds. Once C_{60} molecules reach the bilayer interior, they can facilitate the formation of micropores, which may contribute to the membrane leakage observed in the experiments. We also determined that hydrophilic $C_{60}(OH)_{20}$ molecules, which differ from pristine C_{60}, do not significantly diffuse themselves into the bilayer, and their mean translocation time by Brownian diffusion is approximately 9 orders of magnitude longer. We also discovered that $C_{60}(OH)_{20}$ molecules adsorbed on the membrane surface decrease the spacing between lipid head groups near the adsorption site. These findings highlight the effects of surface functionalization on the interactions between cell membranes and nanomaterials. The demonstrated physical interactions provide a mechanistic explanation of the reduced cytotoxicity of functionalized C_{60} as compared to its pristine form, complementing the chemical mechanisms earlier proposed.

Acknowledgment. We acknowledge the support of an NSF-SGER grant No. BES- 630823. We thank an anonymous reviewer for suggesting an MD simulation to verify the PMF peak of a pristine buckyball located at the bilayer center. We also thank Godfrey Kimball for proofreading the manuscript.

References

(1) Sijbesma, R.; Srdanov, G.; Wudl, F.; Castoro, J. A.; Wilkins, C.; Friedman, S. H.; DeCamp, G. L.; Kenyon, D. L. *J. Am. Chem. Soc.* **1993**, *115*, 6510.
(2) Wharton, T.; Wilson, L. J. *Tetrahedron Lett.* **2002**, *43*, 561.
(3) Ashcroft, J. M.; Tsyboulski, D. A.; Hartman, K. B.; Zakharian, T. Y.; Marks, J. W.; Weisman, R. B.; Rosenblum, M. G.; Wilson, L. J. *ChemComm.* **2006**, *28*, 3004.
(4) Ma, B.; Sun, Y.-P. *J. Chem. Soc., Perkin Trans.* **1996**, *2*, 2157.
(5) Hwang, K. C.; Mauzerall, D. *J. Am. Chem. Soc.* **1992**, *114*, 9705.
(6) Niu, S.; Mauzerall, D. *J. Am. Chem. Soc.* **1996**, *118*, 5791.
(7) Hwang, K. C.; Mauzerall, D. *Nature* **1993**, *361*, 138.
(8) Arbogast, J. W.; Foote, C. S. *J. Am. Chem. Soc.* **1991**, *104*, 2069.
(9) Jeng, U.-S.; Hsu, C. H.; Lin, T.-L.; Wu, C.-M.; Chen, H.-L.; Tai, L.-A.; Hwang, K.-C. *Physica B* **2005**, *357*, 193.
(10) Sayes, C. M.; Fortner, J. D.; Guo, W.; Lyon, D.; Boyd, A. M.; Ausman, K. D.; Tao, Y. J.; Sitharaman, B.; Wilson, L. J.; Hughes, J. B.; et al. *Nano Lett.* **2004**, *4*, 1881.
(11) Chang, R.; Violi, A. *J. Phys. Chem. B* **2006**, *110*, 5073.
(12) Tasseff, R. A.; Kopelevich, D. I. *J. Undergraduate Res., Univ. Florida* **2006**, *7*, 1.
(13) Tieleman, P. http://www.ucalgary.ca/~tieleman/files/dppc128.pdb, 2006.
(14) Tieleman, D. P.; Brerndsen, H. J. C. *J. Chem. Phys.* **1996**, *105*, 4871.
(15) Berger, O.; Edholm, O.; Jahnig, F. *Biophys. J.* **1997**, *72*, 2002.
(16) Rodriguez-Zavala, J. G.; Guirado-Lopez, R. A. *J. Phys. Chem. A* **2006**, *110*, 9459.
(17) Qiao R.; Aluru, N. R. *Nano. Lett.* **2003**, *3*, 1013.
(18) Lindahl, E.; Hess, B.; van der Spoel, D. *J. Mol. Mod.* **2001**, *7*, 306.
(19) Berendsen, H. J. C.; van der Spoel, D.; van Drunen, R. *Comput. Phys. Commun.* **1995**, *91*, 43.
(20) Hess, B.; Bekker, H.; Berendsen, H.; Fraaije, J. *J. Comput. Chem.* **1997**, *18*, 1463.
(21) Humphrey, W.; Dalke, A.; Schulten, K. *J. Mol. Graph.* **1996**, *14*, 33.
(22) Kjellander, R.; Greberg, H. *J. Electroanal. Chem.* **1998**, *450*, 233.
(23) Qiao R.; Aluru, N. R. *Phys. Rev. Lett.* **2004**, *92*, 198301.
(24) Marrink S. J.; Berendsen, H. J. C. *J. Phys. Chem.* **1996**, *100*, 16729.
(25) Gardiner, C. W. *Handbook of Stochastic Methods: For Physics, Chemistry, and the Natural Science*, 2nd ed.; Springer-Verlag: Berlin, 1986.

NL062515F